npj | clean water

www.nature.com/npjcleanwater

ARTICLE OPEN

Check for updates

A hydrate-based zero liquid discharge method for high-concentration organic wastewater: resource recovery and water reclamation

Lingjie Sun[1], Hongsheng Dong[2], Yi Lu[1], Lunxiang Zhang[1,3]✉, Lei Yang[1,3], Jiafei Zhao[1,3]✉ and Yongchen Song[1,3]

High-concentration organic wastewater has become a great challenge for wastewater treatment due to its toxicity and non-biodegradability. Traditional water treatment methods focus on removing or destroying organic pollutants rather than considering the high-concentration organic wastewater as a resource. As an ambitious sustainability goal, resource recovery from wastewater to achieve zero liquid discharge (ZLD) has attracted widespread attention. Here, a hydrate-based method is proposed to treat textile wastewater to facilitate the reuse of dyes and enhance water reclamation. The mechanism of interaction between hydrate and organic pollutants was invested. The results show that organic pollutants are rejected from the growing hydrate lattice and concentrated in the residual solution. This method can achieve a max removal efficiency of 93.6% and a water production rate of 80%. In the range of 0–2000 mg/L, the concentration of organic pollutants does not affect the removal effect and water production rate. The concentrated dye can be reused again. The proposed method exhibits potential for recovering resource and clean water from wastewater while achieving ZLD.

npj Clean Water (2023)6:49 ; https://doi.org/10.1038/s41545-023-00262-w

INTRODUCTION

Wastewater discharged from textile or chemical industries is conventionally characterized by a high concentration of organic pollutants. High-concentration organic wastewater tends to be toxic, carcinogenic, and non-biodegradable. It is hazardous and harmful to the environment and humans[1–3]. Thus, advanced treatment of these high-concentration organic wastewater to achieve water reuse and regeneration will significantly promote sustainable water management[4,5].

The textile industry is one of the primary creators of high-concentration organic wastewater due to its special dyeing operation. Conventional dyeing involves the chemical and physical adsorption of organic dyes on fibers, and these interactions are often weak. Hence, significant dye and water are utilized in the dyeing process[6]. The production of a ton of dyed textiles is estimated to consume more than 200 m^3 of clean water, generating enormous textile wastewater[7,8]. Unfortunately, these low-molecular-weight dyes are easily dissolved and dispersed in water, and separating them from water is very difficult. Therefore, a large amount of unused dye is present in the wastewater[6,9]. Coloring agents in particular are present at high concentrations; these can severely pollute the environment and threaten human health because of their associated toxicity and carcinogenic properties[3,10]. Thus, it is essential to recycle water and dye resources to reduce environmental pollution. Over the past decades, multiple biological, chemical, and physical methods[11–17] (e.g., treatment using microorganisms, oxidation, adsorption, and photocatalysis) have been proposed to treat textile wastewater. Nonetheless, because of the high concentrations and non-biodegradable characteristics of some components in textile wastewater, the treatment to remove these toxic pollutants from textile wastewater is often inadequate[18,19].

In general, textile wastewater has been considered as a waste rather than a resource for reusing dyes and water reclamation[20,21] According to estimates, ~700,000 tons of synthetic dyes are produced annually, but more than 20% of dyes are lost through wastewaters from textile dyeing and finishing because of the low efficiency of the process[22,23]. The recovery of dyes and water from textile wastewater can realize the zero liquid discharge strategy (ZLD) and significantly reduce costs in the dyeing industry and environmental pollution[10,24,25]. However, existing treatment methods focus on the removal or destruction of dyes, which limits their recovery[26,27].

In recent years, membrane technologies and evaporation have been used in wastewater treatment to achieve the near-ZLD of water reclamation and resource recovery[28,29]. Some researchers reported an integrated membrane and thermal-based system for wastewater treatment with near-ZLD and realized the reuse of high-salinity water[30]. Zeng et al. proposed new nanofiltration membranes by adding glycerol as an environmentally friendly co-solvent to enhance the permeability of membranes[31,32]. In spite of these advantages, membranes are inherently sensitive to membrane fouling and scaling, and the accumulating contaminants during wastewater treatment would lead to higher operating pressure, poorer water quality and shorter membrane life. The expensive material cost also limits the large-scale application of membrane technology[33]. Hence, new methods for recovering dyes and water resources from textile wastewater are still urgently needed.

Clathrate hydrates represent ice-like, non-stoichiometric crystalline solid compounds formed through the encapsulation of guest molecules (such as CH_4, CO_2, CCl_2FCH_3) in a cage-like skeleton of hydrogen-bonded water molecules, under high pressure or low temperature conditions[34,35]. Natural gas hydrates are wildly found

[1]Key Laboratory of Ocean Energy Utilization and Energy Conservation of Ministry of Education, School of Energy and Power Engineering, Dalian University of Technology, 116024 Dalian, China. [2]Dalian National Laboratory for Clean Energy, Dalian Institute of Chemical Physics, Chinese Academy of Sciences, 116023 Dalian, China. [3]Ningbo Institute of Dalian University of Technology, 315016 Ningbo, China. ✉email: lunxiangzhang@dlut.edu.cn; jfzhao@dlut.edu.cn

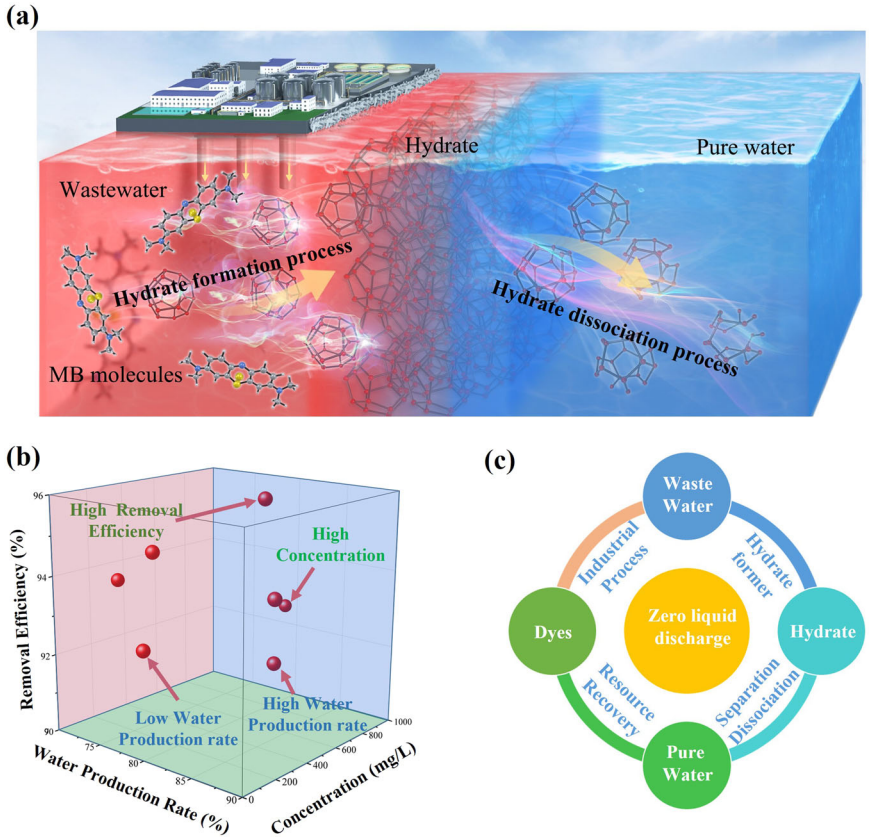

Fig. 1 Hydrate as a wastewater treatment material. a Schematic diagram of the wastewater treatment process, where liquid water molecules were converted into solid hydrates. And the pure solid hydrate after solid–liquid separation can be decomposed to produce fresh water. **b** Performance of the treatment via hydrate method. The front panel represents a high removal efficiency and water production rate. The right panel depicts a high-concentration treatment capacity. **c** Schematic diagram of the system used for experiments.

in continental margins and beneath permafrost regions[36,37]; one volume of hydrate can disassociate into 164 volumes of methane at standard temperature and pressure[38]. Thus, they are also considered an enormous potential energy resource. During the hydrate formation process, guest molecules with specific size can be enclathrated in a cage-like skeleton, converting liquid water into solid hydrates. Reversibly, the pure solid hydrate can be decomposed into pure water and guest molecules again via heating or depressurization[38,39]. Due to the unique feature of hydrate, the hydrate-based technologies have attracted much attention and become a hot topic in recent years in desalination[40], gas storage[41], cold storage[42], gas separation, and even CO_2 capture for net-zero emissions[43].

The schematic diagram of the wastewater treatment process is shown in Fig. 1. The unique structure and chemical properties of hydrates make hydrates have the potential to achieve ZLD in wastewater treatment. Compared with thermal evaporation and membrane distillation, the latent heat of CCl_2FCH_3 (R141b) hydrates is 344 kJ/kg which is smaller than that of water (2444 kJ/kg)[44–46], so the energy consumption of hydrate formation is lower than thermal evaporation and membrane distillation. On the other hand, the membrane synthesis process is complex, while the wastewater treatment using the hydrate method is simple and maneuverable. Membrane distillation processes also need further development with emphasis on energy efficiency, lower temperature and concentration polarizations[47,48]. However, few studies focus on the behavior of hydrate formation in organic solution because of the high concentrations and complexity of such components emanating. Furthermore, the interaction between organic contaminants and hydrate cages is unclear, which limits the application of the hydrate wastewater treatment technology.

In the present study, a hydrate-based method for the recovery of dyes and water from textile wastewater was proposed. This study provides an avenue to recycle raw materials and realize ZLD. It could be regarded as an environmentally friendly approach for treating textile wastewater. The mechanism and characteristics of the exclusion during hydrate formation in dye-containing wastewater were simulated to further understand the interaction between organic dye molecules and hydrate cages. The effects of the concentration of the dye and the hydrate formation time on wastewater treatment were also studied. The hydrate technology is promising for the treatment of dye-containing wastewater and purification in other industries, such as the food and pharmaceutical industries.

RESULTS AND DISCUSSION

Exclusion mechanism during the hydrate formation process

During the hydrate formation process, water molecules form cage skeletons through hydrogen bonds in which guest molecules become trapped. The other solutes are rejected from the growing hydrate lattice and concentrated in the residual solution. This process is termed hydrate exclusion effect. Although previous studies indicated that inorganic molecules (such as $Na+$, $Cl-$) are excluded from the lattice during the hydrate formation process[49–51], it is still not clear whether some organic molecules such as methylene blue (MB) could be excluded from the cages of the growing hydrate crystals. The exclusion mechanism during the formation process remains controversial.

To understand the mechanism and characteristics of hydrate formation in a solution containing MB, molecular dynamics

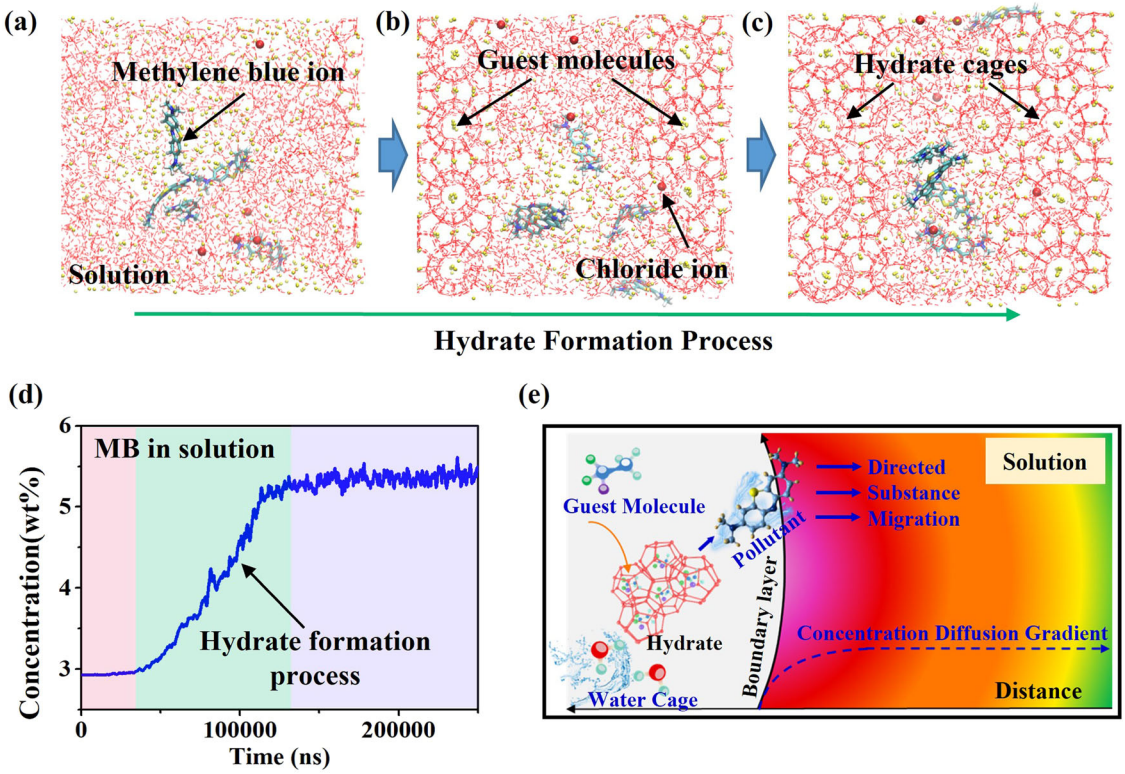

Fig. 2 Illustration of the exclusion effect during the hydrate formation process in dye-containing wastewater. a–c depict the hydrate formation process. **a** Initial stage of the simulation: MB molecules are dispersed in the solution. **b** Nucleation occurred and solid hydrate was formed; the MB molecules were excluded from the hydrate cage skeletons. **c** More water molecules turned into solid hydrate and more MB molecules were gradually enriched in the solution. **d** Variation in the MB concentration in the solution during the simulation process of hydrate formation. **e** Schematic diagram of MB diffusion into the solution from the hydrate formation boundary layer due to the exclusion effect during hydrate formation.

simulations were performed. As shown in Fig. 2a–c, during the hydrate formation process, the cage structures were continuously formed, and the guest molecules are encapsulated in the cage structures. On the contrary, MB molecules were rejected from the growing hydrate lattice, and this caused enrichment of MB in the residual solution. In Fig. 2d, the increase in the MB concentration in the residual solution also confirmed the existence of the hydrate exclusion effect. The accumulation of massive MB molecules excluded from hydrate cage skeletons leads to an increase in the MB concentration at the hydrate boundary layer. Thereafter, the high concentration of MB at the hydrate boundary layer gradually diffuses into the solution and forms a concentration gradient (Fig. 2e)[52]. These results imply that the hydrate obtained after the separation contained just water and guest molecules. Thus, clean water production is possible after the dissociation, and this highlights the feasibility of regenerating dyes and water for resource reclamation from textile wastewater using the hydrate method.

The Raman spectra of MB in dw, R141b, the hydrate formed in dw, and the hydrate formed in the MB aqueous solution (aq) are displayed in Fig. 3. Regarding the MB aqueous solution, peaks are observed at 450.12, 502.10, 1400.96, and 1625.98 cm^{-1}, and the largest peak is assigned to stretching vibrations of the C–C band. Relatedly, the peaks at 450.12 and 502.10 cm^{-1} are associated with the bending of the C–N–C skeleton, whereas the peak at 1400.96 cm^{-1} is attributed to the (C–H) in-plane ring deformation[53,54]. The pure liquid R141b has a prominent peak at 589.19 cm^{-1} and the peak was also found in the hydrate formed in dw and the MB solution. Nevertheless, these MB vibration peaks are missing in the spectrum of the hydrate formed in the MB solution. These results demonstrate that molecules of the MB were excluded from the structure of the hydrate during its formation. This could be explained that the size of MB molecules was 1.38 nm, which was larger than that of hydrate cages (0.39–0.57 nm)[38,55]. In addition, the crystal structures of hydrate formed in dw and MB solution were also analyzed. According to previous studies, the R141b forms the sII hydrate[56]. Typical PXRD patterns of the sII hydrate and ice Ih[57] are depicted in red and blue in Fig. 3c. The PXRD results show that hydrates formed in dw and MB solution are cubic sII hydrate with the space group Fd3m. The peak attributed to ice also displays its maximum intensities in the two samples. The intensity of the ice peak corresponded to the amount of residual water after the centrifugation. These PXRD results demonstrate that the structure of the R141b hydrate was unaffected by the MB molecules.

Effects of hydrate formation characteristics on wastewater treatment

According to the chemical reaction equation of ref. [56], the volumetric ratio of water to R141b needed to completely convert the water molecules into hydrate is 3.5. As the amount of R141b increases, the centrifugal removal efficiency decreases, whereas the water production rate decreases as the amount of R141b declines. Thus, in the present study[52], the optimum volumetric ratio of water to R141b was found to be 4. As the formation time increased, the hydrate morphology changed from a suspension to a slurry, and then to a block. After a formation duration of approximately 11 h, the hydrate retained a block morphology, and the strength of the hydrate block increased as time increased. The images of hydrate morphology at different times could be found in Supplementary Fig. 1.

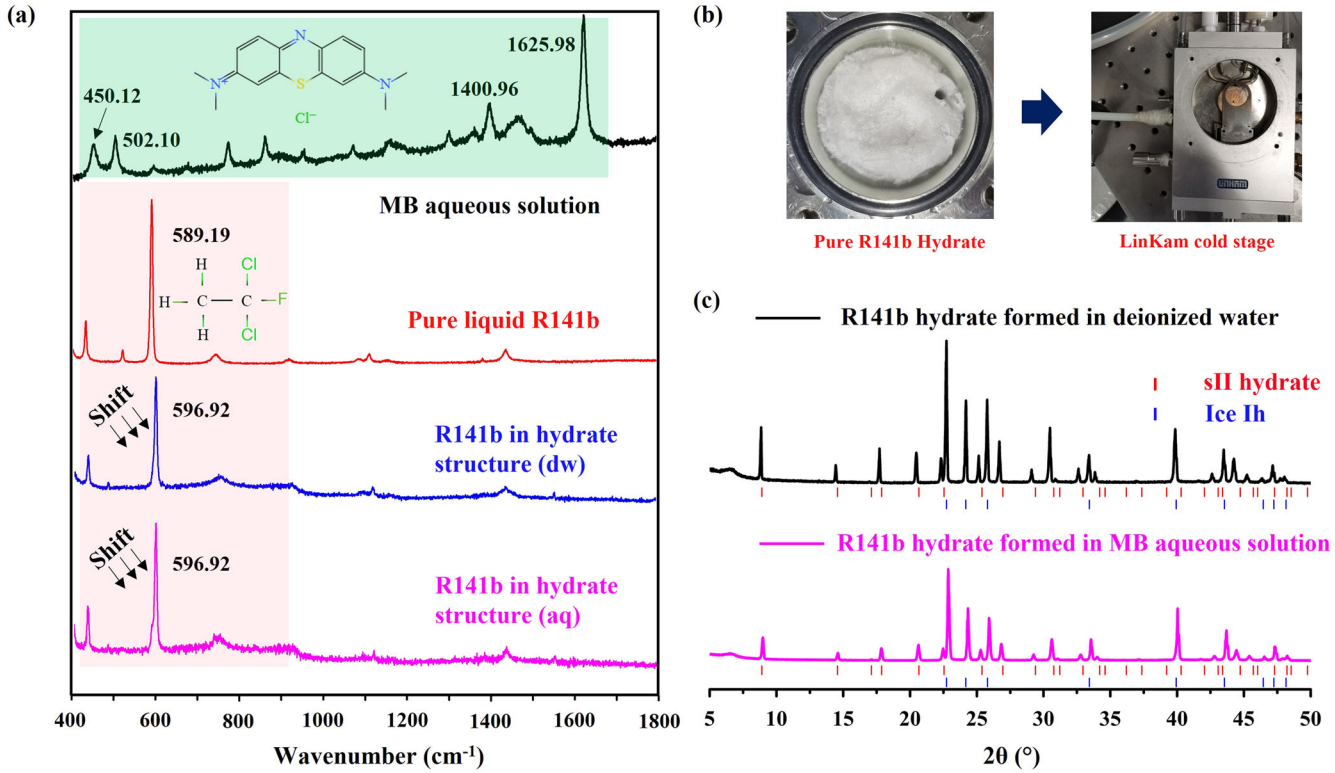

Fig. 3 Raman spectra of the MB aqueous solution, liquid R141b, and hydrates. a Raman spectra of an MB aqueous solution with a concentration of 2000 mg/L. The main characteristic Raman peaks of MB are at 1625.98 cm^{-1}, 1400.96 cm^{-1}, 502.10 cm^{-1}, and 450.12 cm^{-1}. The characteristic Raman peak of liquid R141b is at 589.19 cm^{-1}. The characteristic peak of R141b in hydrate formed in deionized water and MB aqueous solution both are at 596.92 cm^{-1}. **b** Pure R141b hydrate and the LinKam cold stage for Raman analysis. **c** The PXRD patterns of R141b hydrate formed in deionized water and MB aqueous solution.

After hydrate formation, a solid–liquid separation was conducted via a vacuum filtration or centrifugation. The dye removal efficiencies, water production rates, and enrichment factors associated with different hydrate formation times are displayed in Fig. 4. The removal efficiency related to centrifugation was stable at ~90%, and this indicates that the formation time minimally affected the efficiency. Nevertheless, regarding vacuum filtration, the removal efficiency decreased from 51.1 to 31.7% as the hydrate formation time increased. Owing to the increased strength of the hydrate block as the formation time increased, small amounts of the residual liquid were trapped and isolated between particles of the hydrate. Thus, the separation of the residual liquid from the hydrate through vacuum filtration was difficult. The release of these residual liquid pockets after the decomposition of the hydrate explains the lower efficiency of the vacuum filtration[52,58].

As the hydrate formation time increases, the conversion of water to hydrate increases. The water production rate changed from 48.5% to 78.1% as the formation time increased from 3 to 24 h. Relatedly, dye molecules were further concentrated in the residual liquid, and thus the enrichment factor increased from 1.34 to 1.78. Although the water production rate and enrichment factor were elevated as the formation time increased, the difficulty involved in the hydrate-residual liquid separation was also enhanced. Consequently, to improve the removal efficiency, effective separation of the hydrate from the residual liquid is vital.

Controlling factors and optimization of the wastewater treatment procedure

Despite the high efficiency of the hydrate-residual liquid separation linked to the centrifugation, the energy consumption is considerably high[59]. To understand the factors controlling the separation and to optimize the treatment procedure accordingly, hydrate particles formed at different times were analyzed, and the results are shown in Fig. 5. As the formation time increased from 1 to 10 h, the hydrate particles remained between 5.8–7.7 μm (Fig. 5e, f), but the amount of hydrate increased from 20.5 g to 36.4 g.

As displayed in Fig. 5a–d, the removal efficiency linked to centrifugation was stable at ~90%, whereas that related to the vacuum filtration decreased from 62.6% to 19.2% as the amount of hydrate increased. Meanwhile, both the water production rate and the enrichment factor increased. These results demonstrate that the residual pockets of liquid were linked to the increased amount of hydrate instead of the size of the hydrate particles. Therefore, controlling the amount of hydrate is crucial for the enhancement of the removal efficiency and optimization of the treatment procedure. According to experimental data, a formation time varying between 6 and 8 h is optimal because the slurry hydrate is easier to filter. Thus, a higher removal efficiency can be obtained through centrifugation. If the formation time exceeds 10 h, the morphology of the hydrate is a block. Evidently, the formation time minimally affected the water production rate and the enrichment factor, but it negatively impacted the removal efficiency and energy consumption.

Suitability of the hydrate method for varying initial concentrations of MB

Figure 6 shows the impact of the initial concentration of MB on the characteristics of its removal. As the concentration of MB increased from 101.9 to 982.6 mg/L, the removal efficiency via centrifugation remained between 92.4 and 96.2%. Conversely, the concentration of MB in the liquid pockets trapped in the hydrate and the amount of MB adsorbed on the surface of the

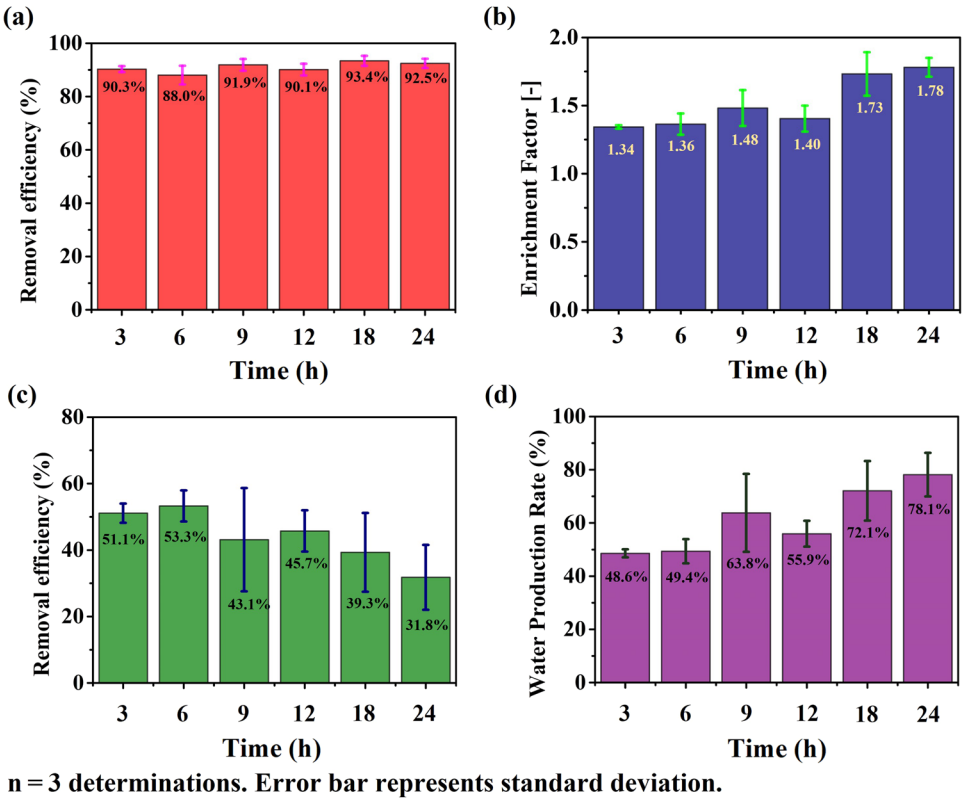

Fig. 4 The effect of the hydrate formation time on wastewater treatment. a Removal efficiency via centrifugation, **b** enrichment factor, **c** removal efficiency through vacuum filtration, and **d** water production rate. Conditions: initial concentration of MB = 101.9 mg/L. Each experiment was repeated three times ($n = 3$). Error bar represents standard deviation.

hydrate increased as the initial concentration of MB increased. Consequently, the removal efficiency through vacuum filtration decreased, whereas the water production rate and the enrichment factor remained stable at ~80% and 1.7, respectively. Compared with that seen using traditional methods, the hydrate method is unaffected by the concentration of the dye, and it exhibits extensive adaptability. The dissociation water could be recovered and reused. Following several cycles of hydrate formation and decomposition, even pure water could be obtained. The highest enrichment factor is 2.17 in Fig. 6b. It meant that although the initial concentration in wastewater is 398.2 mg/L, the concentration in concentrated solution could reach 864.1 mg/L. Thus, it is easier to recover dyes further from concentrated solution by adsorption, nanofiltration or other methods[60,61].

Therefore, we proposed a hydrate-based ZLD strategy for industrial wastewater treatment as illustrated in Fig. 7. First, the wastewater from the dyeing factory and R141b are transported into the hydrate formation system. The temperature in the hydrate formation system maintains below 281.55K[52] to promote hydrate formation at atmospheric pressure. Then, water molecules and R141b molecules are converted into solid hydrate. After hydrate formation, filtration is conducted to separate the solid hydrate and residual liquid. After that, solid hydrate is placed in a centrifuge to further remove interstitial water. Finally, pure hydrate is dissociated into water and R141b in the dissociation system. Then, the treated water could be obtained and recycled again. The R141b can also be reused. The residual concentrated solution is rich in the dye, so it is easier to further recover dyes from the concentrated solution by adsorption, nanofiltration or other methods to reduce dye consumption[60,61]. It is estimated that more than 140,000 dyes are lost through wastewater from textile dyeing and finishing[22,23]. The hydrate method has the potential as an alternative to conventional textile wastewater treatment to realize resource recovery and water reclamation.

To further evaluate the economic cost of a hydrate-based wastewater treatment system, we conducted thermodynamic calculations to obtain the energy consumption and analysis the operation costs. The economic cost of a hydrate-based wastewater treatment system was compared with other method wastewater treatment methods in Table 1.

Conventional water production costs from wastewater recovery and reuse typically lie in the range between 0.20 and 1.26 $/t[62–64], depending on which level the treatment is initiated and the treatment level required for its reuse[64]. For membrane-based processes for wastewater recovery such as reverse osmosis or membrane distillation system, the quality of treated water is higher than that of conventional wastewater methods. Still, the cost is also higher than conventional wastewater and the membrane fouling and scaling remain challenges[65,66]. In this manuscript, the hydrate method is unaffected by the concentration of the dye, and it exhibits extensive adaptability. The cost of the hydrate method is 2.28 $/t, which is lower than that of thermal evaporation and membrane distillation. The results demonstrated that the hydrate method showed a high potential in industrial application.

In summary, we report a hydrate-based ZLD method for the treatment of textile wastewater for the recovery of dyes and reuse of water[52]. Different from the conventional methods that involve destroying dyes to realize wastewater purification, the hydrate-based method directly extracts water molecules from wastewater. In the process of hydrate formation, water molecules form cage skeletons through hydrogen bonds; only hydrate-forming molecules can be trapped in the cage skeletons. The contaminant can thus be excluded from the growing hydrate lattice and enriched in the residual solution. Pure water could be obtained by dissociation of the solid hydrate. The dye contaminants enriched in the

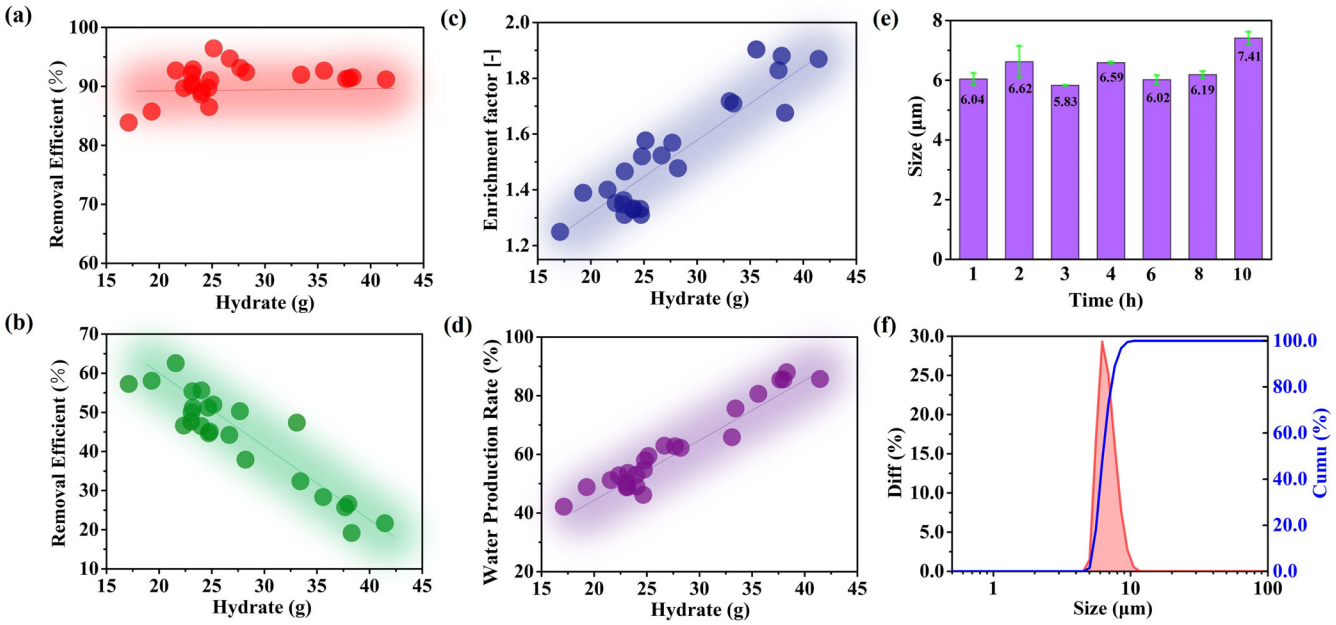

Fig. 5 Plots showing the effects of the amount of hydrate on wastewater treatment. a Removal efficiency via centrifugation, **b** enrichment factor, **c** removal efficiency vacuum filtration, and **d** water production rate. **e**, **f** Size of the hydrate particles associated with different formation times.

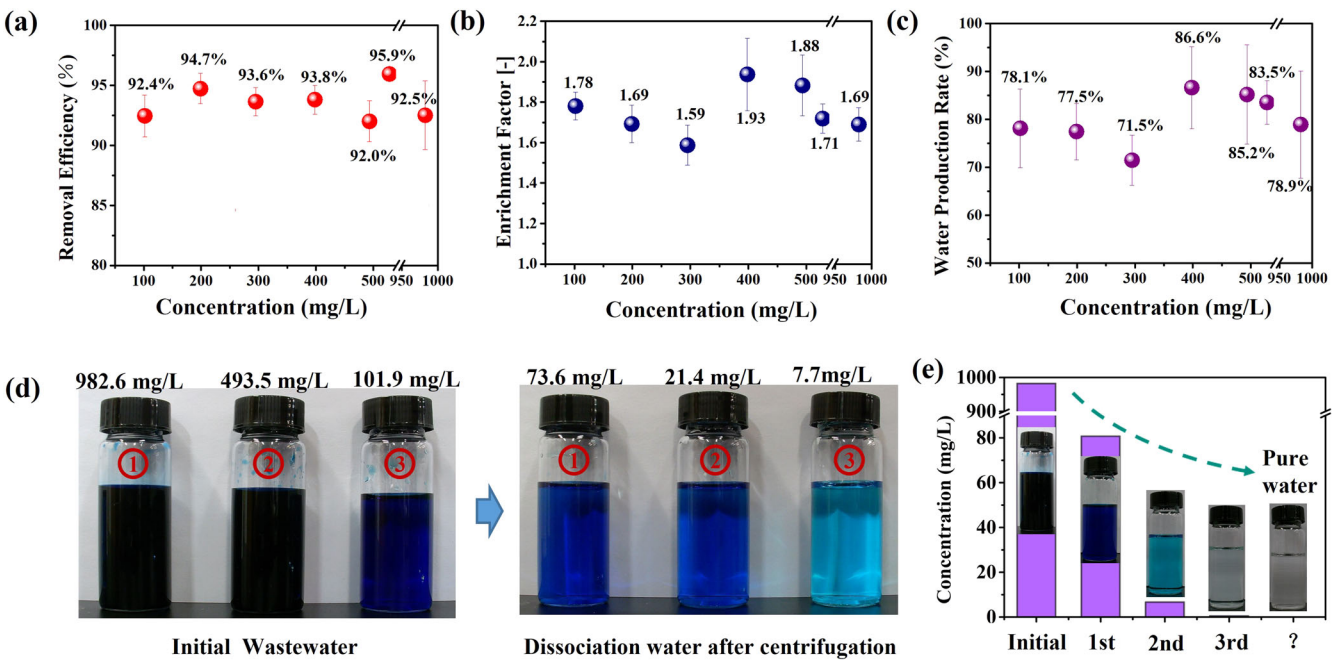

n = 3 determinations. Error bar represents standard deviation.

Fig. 6 Plots displaying the effects of the initial concentration of MB on wastewater treatment. a Removal efficiency via centrifugation, **b** water production rate, and **c** enrichment factor. **d** Images of wastewater samples with different concentrations and the dissociation water after centrifugation. **e** MB concentration of the dissociation water after each hydrate reformation and dissociation. Conditions: initial concentration of MB from 101.9 to 982.6 mg/L. Each experiment was repeated three times ($n = 3$). Error bar represents standard deviation.

residual solution can also be reused by simple green routes. More remarkably, hydrate can also form at high dye concentrations in wastewater, a unique feature in comparison to the capabilities of other traditional methods. The outcomes of this study demonstrate the strong potential for water reclamation and resource recovery in wastewater treatment as well as desalination, food, and medical dehydration purification applications.

METHODS

Experimental materials and apparatus

The methylene blue utilized was purchased from J & K Scientific, Beijing, P.R.C. The hydrochlorofluorocarbon (R141b) was acquired from Juhua Group Corporation, Zhejiang Province, P.R.C, whereas deionized water (dw) was obtained from a

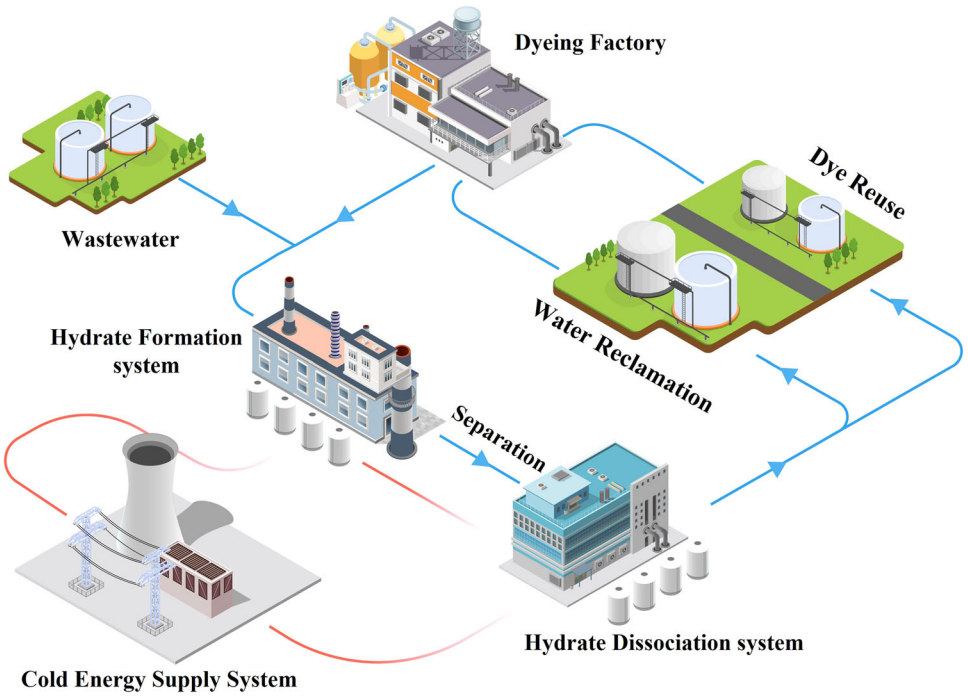

Fig. 7 Industrial flowsheet using hydrate-based technology for resource recovery and water reclamation from wastewater. Clathrate hydrate-based dye-containing wastewater treatment which is characterized by zero liquid discharge.

Table 1. The cost comparison of different wastewater treatment methods.

Technology	Operating and maintenance costs ($/m^3)	Reference
Activated sludge	0.2–1.26	62–64
Membrane bioreactor	0.48–2.29	63,67,68
Seawater reverse osmosis	2–4.5	69
Membrane distillation	10–16	70
Propane hydrate	2.76–4.23	71
This work	2.28	–

water purification system in the lab. A hydrate reactor with an internal volume of 200 mL was used to form hydrate. The temperature of the reactor was controlled using a water bath (F38-EH, JULABO Inc., Germany).

Hydrate formation and separation procedure

Before the experiment, 40 g of simulated wastewater and 13.3 g of R141b were added to the reactor. Then the reactor was put into the water bath. The temperature of the water bath was maintained at 275.15 K. Then, the temperature of the reactor was decreased to 275.15 K to form hydrate. A magnetic stirrer was used to promote the nucleation of hydrate.

Following the completion of the hydrate formation, vacuum filtration was conducted to separate the solid hydrate and residual liquid. Then, solid hydrate was placed in a centrifuge and centrifuged at 3000 rpm for 3 min to further remove interstitial water. After separation, the hydrate was transferred to a decomposer, where the hydrate decomposed into water and R141b at 293 K and atmospheric pressure. Then the R141b could be separated from the R141b-water mixture based on its immiscibility with water. Finally, the R141b was collected and reused. The residual solution obtained through vacuum filtration or centrifugation also contained reconcentrated dye, which can be reused in dye production and textile dyeing. More details could be found in our previous work[52,66].

Analysis of samples

The absorption spectra of wastewater were recorded by using a UV–Vis–NIR spectrophotometer (Lambda750S, USA). Calibration was performed to establish the relationship between the UV absorption intensity and the concentration of MB.

To clarify the mechanism and characteristics of the exclusion and understand the effect of the dye on the structure of the hydrate and the distribution of guest molecules in the cage, hydrate samples produced in dw and the simulated wastewater were characterized via powder X-ray diffraction (PXRD, D8 ADVANCE, Bruker, German) and Raman spectroscopy.

Efficiency, enrichment, and production rate calculation

Based on the concentrations of MB measured, the removal efficiency, enrichment factor, and water production rate were calculated as follows:

$$\text{Removal Efficiency} = \frac{C_i - C_d}{C_i} \times 100\% \quad (1)$$

where C_i and C_d are the concentrations of MB in the simulated wastewater and water from the decomposition. The C_d includes water obtained from decomposition through vacuum filtration or centrifugation.

$$\text{Enrichment Factor} = \frac{C_r}{C_i} \quad (2)$$

where C_r is the concentration of MB in a concentrated solution.

$$\text{Water Production Rate} = \frac{V_i - V_r}{V_i} \times 100\% \quad (3)$$

where V_i is the initial volume of simulated wastewater in the reactor and V_r is the volume of the residual solution after vacuum filtration or centrifugation.

DATA AVAILABILITY

The data that support the findings of this study are available from the corresponding author upon reasonable request.

Received: 8 October 2022; Accepted: 15 June 2023;
Published online: 28 June 2023

REFERENCES

1. Yang, B., Zhang, L., Lee, Y. & Jahng, D. Novel bioevaporation process for the zero-discharge treatment of highly concentrated organic wastewater. *Water Res.* **47**, 5678–5689 (2013).
2. Qin, D., Liu, Z., Liu, Z., Bai, H. & Sun, D. Superior antifouling capability of hydrogel forward osmosis membrane for treating wastewaters with high concentration of organic foulants. *Environ. Sci. Technol.* **52**, 1421–1428 (2018).
3. Wang, X., Liu, K., Qang, Z., Heng, L. & Jiang, L. A robust and renewable solar steam generator for high concentration dye wastewater purification. *J. Mater. Chem. A.* **10**, 3436–3442 (2022).
4. Mukherjee, A. et al. Paradigm shift toward developing a zero liquid discharge strategy for dye-contaminated water streams: a green and sustainable approach using hydrodynamic cavitation and vacuum membrane distillation. *ACS Sustain. Chem. Eng.* **9**, 6707–6719 (2021).
5. Hoekstra, A. Y. Water scarcity challenges to business. *Nat. Clim. Change* **4**, 318–320 (2014).
6. Ding, X. et al. A promising clean way to textile colouration: cotton fabric covalently-bonded with carbon black, cobalt blue, cobalt green, and iron oxide red nanoparticles. *Green. Chem.* **21**, 6611–6621 (2019).
7. Güyer, G. T., Nadeem, K. & Dizge, N. Recycling of pad-batch washing textile wastewater through advanced oxidation processes and its reusability assessment for Turkish textile industry. *J. Clean. Prod.* **139**, 488–494 (2016).
8. Jiang, M. et al. Conventional ultrafiltration as effective strategy for dye/salt fractionation in textile wastewater treatment. *Environ. Sci. Technol.* **52**, 10698–10708 (2018).
9. Blackburn, R. S. & Burkinshaw, S. M. A greener approach to cotton dyeings with excellent wash fastness. *Green. Chem.* **4**, 47–52 (2002).
10. Chen, Q. et al. Comparative study on the treatment of raw and biologically treated textile effluents through submerged nanofiltration. *J. Hazard. Mater.* **284**, 121–129 (2015).
11. Adam, A. et al. Ion-capture electrodialysis using multifunctional adsorptive membranes. *Science* **372**, 296–299 (2021).
12. Xu, J. et al. Organic wastewater treatment by a single-atom catalyst and electrolytically produced H_2O_2. *Nat. Sustain* **4**, 233–241 (2021).
13. Johnson, J. K. et al. Removing forever chemicals via amphiphilic functionalized membranes. *NPJ Clean. Water* **5**, 55 (2022).
14. Petcu, A. R. et al. No catalyst dye photodegradation in a microemulsion template. *ACS Sustain. Chem. Eng.* **5**, 5273–5283 (2017).
15. Fanourakis, S. K., Peña-Bahamonde, J., Bandara, P. C. & Rodrigues, D. F. Nano-based adsorbent and photocatalyst use for pharmaceutical contaminant removal during indirect potable water reuse. *NPJ Clean. Water* **3**, 1 (2020).
16. Han, G., Feng, Y., Chung, T. S., Weber, M. & Maletzko, C. Phase inversion directly induced tight ultrafiltration (UF) hollow fiber membranes for effective removal of textile dyes. *Environ. Sci. Technol.* **51**, 14254–14261 (2017).
17. Peng, C. et al. Graphene-templated formation of two-dimensional lepidocrocite nanostructures for high-efficiency catalytic degradation of phenols. *Energy Environ. Sci.* **4**, 2035–2040 (2011).
18. Ahmed, M. et al. Recent developments in hazardous pollutants removal from wastewater and water reuse within a circular economy. *NPJ Clean. Water* **5**, 12 (2022).
19. Grant, S. et al. Taking the "waste" out of "wastewater" for human water security and ecosystem sustainability. *Science* **337**, 681–686 (2012).
20. McCarty, P. L., Bae, J. & Kim, J. Domestic wastewater treatment as producer a net energy. can this be achieved? *Environ. Sci. Technol.* **45**, 7100–7106 (2011).
21. Logan, B. E. & Elimelech, M. Membrane-based processes for sustainable power generation using water. *Nature* **488**, 313–319 (2012).
22. Gunay, M. *Eco-Friendly Textile Dyeing and Finishing* (BoD–Books on Demand, 2013).
23. Haslinger, S., Wang, Y., Rissanen, M., Lossa, M. B. & Sixta, H. Recycling of vat and reactive dyed textile waste to new colored man-made cellulose fibers. *Green. Chem.* **21**, 5598–5610 (2019).
24. Wang, C., Chen, Y., Hu, X. & Feng, X. In-situ synthesis of PA/PVDF composite hollow fiber membranes with an outer selective structure for efficient fractionation of low-molecular-weight dyes-salts. *Desalination* **503**, 114957 (2021).
25. Hilal, N. & Wright, C. J. Exploring the current state of play for cost-effective water treatment by membranes. *NPJ Clean Water*. **1**, 8 (2018).
26. Shen, Z. et al. Dual electrodes oxidation of dye wastewater with gas diffusion cathode. *Environ. Sci. Technol.* **39**, 1819–1826 (2005).
27. Chethana, M., Sorokhaibam, L., Bhandari, V., Raja, S. & Ranade, V. Green approach to dye wastewater treatment using biocoagulants. *ACS Sustain. Chem. Eng.* **4**, 2495–2507 (2016).
28. Shah, V., Wang, B. & Li, K. High-performance PVDF membranes prepared by the combined crystallisation and diffusion (CCD) method using a dual-casting technique: a breakthrough for water treatment applications. *Energy Environ. Sci.* **14**, 5491–5500 (2021).
29. Wang, Z., Deshmukh, A., Du, Y. & Elimelech, M. Minimal and zero liquid discharge with reverse osmosis using low-salt-rejection membranes. *Water Res.* **170**, 115317 (2020).
30. Menon, A., Haechler, I., Kaur, S., Lubner, S. & Prasher, R. S. Enhanced solar evaporation using a photo-thermal umbrella for wastewater management. *Nat. Sustain.* **3**, 144–151 (2020).
31. Zeng, H. et al. Green glycerol tailored composite membranes with boosted nanofiltration performance. *J. Membr. Sci.* **663**, 121064 (2022).
32. Yang, F. et al. Unprecedented acid-tolerant ultrathin membranes with finely tuned sub-nanopores for energetic-efficient molecular sieving. *Sci. Bull.* **68**, 29–33 (2023).
33. Goh, P. & Ismail, A. A review on inorganic membranes for desalination and wastewater treatment. *Desalination* **434**, 60–80 (2018).
34. Sloan, E. D. Fundamental principles and applications of natural gas hydrates. *Nature* **426**, 353–359 (2003).
35. Walsh, M. et al. Microsecond simulations of spontaneous methane hydrate nucleation and growth. *Science* **326**, 1095–1098 (2009).
36. Boswell, R. & Collett, T. S. Current perspectives on gas hydrate resources. *Energy Environ. Sci.* **4**, 1206–1215 (2011).
37. Zhu, J. et al. Encapsulation kinetics and dynamics of carbon monoxide in clathrate hydrate. *Nat. Commun.* **5**, 4128 (2014).
38. Sloan, E. D. & Koh, C. A. *Clathrate Hydrates of Natural Gases*, Third edn. (CRC Press/Taylor & Francis, 2008).
39. Yu, X. et al. Crystal structure and encapsulation dynamics of ice II-structured neon hydrate. *Proc. Natl Acad. Sci. USA* **111**, 10456–10461 (2014).
40. Montazeri, S. M. & Kolliopoulos, G. Hydrate based desalination for sustainable water treatment: a review. *Desalination* **537**, 115855 (2022).
41. Sun, L. et al. Enhanced clathrate hydrate formation at ambient temperatures (287.2 K) and near atmospheric pressure (0.1 MPa): application to solidified natural gas technology. *Chem. Eng. J.* **454**, 140325 (2023).
42. Cheng, C. et al. Review and prospects of hydrate cold storage technology. *Renew. Sustain. Energy Rev.* **ume 117**, 109492 (2020).
43. Ndlovu, P., Babaee, S. & Naidoo, P. Review on CH_4-CO_2 replacement for CO_2 sequestration and CH_4/CO_2 hydrate formation in porous media. *Fuel* **320**, 123795 (2022).
44. Bi, Y., Guo, T., Zhu, T., Zhang, L. & Chen, L. Influences of additives on the gas hydrate cool storage process in a new gas hydrate cool storage system. *Energy Convers. Manag* **47**, 2974–2982 (2006).
45. Wang, X., Dennis, M. & Hou, L. Clathrate hydrate technology for cold storage in air conditioning systems. *Renew. Sust. Energy. Rev.* **36**, 34–51 (2014).
46. Tang, J. et al. Realization of low latent heat of a solar evaporator via regulating the water state in wood channels. *ACS Appl. Mater. Interfaces* **12**, 18504–18511 (2020).
47. Shirazi, M. M. A. & Dumée, L. F. Membrane distillation for sustainable wastewater treatment. *J. Water Process. Eng.* **47**, 102670 (2022).
48. Xu, D., Zhu, Z. & Li, J. Recent progress in electrospun nanofibers for the membrane distillation of hypersaline wastewaters. *Adv. Fiber Mater.* **4**, 1357–1374 (2022).
49. Yagasaki, T., Matsumoto, M. & Tanaka, H. Adsorption of kinetic hydrate inhibitors on growing surfaces: a molecular dynamics study. *J. Phys. Chem. B.* **122**, 3396–3406 (2018).
50. Wren, S. N. & Donaldson, D. J. Exclusion of nitrate to the air–ice interface during freezing. *Phys. Chem. Lett.* **2**, 1967–1971 (2011).
51. Philip, P., Chakraborty, S. & Kahan, T. F. Physical characterization of frozen salt-water solutions using Raman microscopy. *ACS Earth Space Chem.* **2**, 702–710 (2018).
52. Dong, H., Zhang, L., Ling, Z., Zhao, J. & Song, Y. The controlling factors and ion exclusion mechanism of hydrate-based pollutant removal. *ACS Sustain. Chem. Eng.* **7**, 7932–7940 (2019).
53. Hassanpouryouzband, A. et al. Gas hydrates in sustainable chemistry. *Chem. Soc. Rev.* **49**, 5225–5309 (2020).
54. Xiao, G. & Man, S. Surface-enhanced Raman scattering of methylene blue adsorbed on cap-shaped silver nanoparticles. *Phys. Lett.* **447**, 305–309 (2007).

55. Wang, C., Li, J., Lv, X., Zhang, Y. & Guo, G. Photocatalytic organic pollutants degradation in metal–organic frameworks. *Energy Environ. Sci.* **7**, 2831–2867 (2014).
56. Li, J., Guo, K., Liang, D. & Wang, R. Experiments on fast nucleation and growth of HCFC141b gas hydrate in static water columns. *Int. J. Refrig.* **27**, 932–939 (2004).
57. Lee, Y. et al. Structural transition induced by cage-dependent guest exchange in $CH_4 + C_3H_8$ hydrates with CO_2 injection for energy recovery and CO_2 sequestration. *Appl. Energy* **228**, 229–239 (2018).
58. Park, K. et al. A new apparatus for seawater desalination by gas hydrate process and removal characteristics of dissolved minerals (Na^+, Mg^{2+}, Ca^{2+}, K^+, B^{3+}). *Desalination* **274**, 91–96 (2011).
59. Martínez, J. et al. Techno-economic analysis of a membrane-hybrid process as a novel low-energy alternative for zero liquid discharge systems. *Energy Convers. Manag.* **211**, 112783 (2020).
60. Wang, P., Wang, P., Guo, Y., Rao, L. & Yan, C. Selective recovery of protonated dyes from dye wastewater by pH-responsive BCN material. *Chem. Eng. J.* **412**, 128532 (2021).
61. Lin, J. et al. Toward resource recovery from textile wastewater: dye extraction, water and base/acid regeneration using a hybrid NF-BMED process. *ACS Sustain. Chem. Eng.* **3**, 1993–2001 (2015).
62. Arif, A., Sorour, M. & Aly, S. Cost analysis of activated sludge and membrane bioreactor WWTPs using CapdetWorks simulation program: case study of Tikrit WWTP (middle Iraq). *Alex. Eng. J.* **59**, 4659–4667 (2020).
63. Guo, T., Englehardt, J. & Wu, T. Review of cost versus scale: water and wastewater treatment and reuse processes. *Water Sci. Technol.* **69**, 223–34 (2014).
64. Linares, R. et al. Life cycle cost of a hybrid forward osmosis—low pressure reverse osmosis system for seawater desalination and wastewater recovery. *Water Res.* **88**, 225–234 (2016).
65. Xie, M., Shon, H., Gray, S. & Elimelech, M. Membrane-based processes for wastewater nutrient recovery: Technology, challenges, and future direction. *Water Res.* **89**, 210–221 (2016).
66. Tong, T. & Elimelech, E. The global rise of zero liquid discharge for wastewater management: drivers, technologies, and future directions. *Environ. Sci. Technol.* **50**, 6846–55 (2016).
67. Suárez, A., Fernández, P., Iglesias, J., Iglesias, E. & Riera, F. Cost assessment of membrane processes: a practical example in the dairy wastewater reclamation by reverse osmosis. *J. Membr. Sci.* **493**, 389–402 (2015).
68. Judd, S. J. Membrane technology costs and me. *Water Res.* **122**, 1–9 (2017).
69. Gude, V. G. Desalination and sustainability—an appraisal and current perspective. *Water Res.* **89**, 87–106 (2016).
70. Bartholomew, T., Dudchenko, A., Siefert, N. & Mauter, M. Cost optimization of high recovery single stage gap membrane distillation. *J. Membr. Sci.* **611**, 118370 (2020).
71. Javanmardi, J. & Moshfeghian, M. Energy consumption and economic evaluation of water desalination by hydrate phenomenon. *Appl. Therm. Eng.* **23**, 845–857 (2003).

ACKNOWLEDGEMENTS

This study was supported by the National Natural Science Foundation of China (Grant Nos. 52020105007, 52025066, 52006024, U21B2065) and the Fundamental Research Funds for the Central Universities (Grant No. DUT22LAB130).

AUTHOR CONTRIBUTIONS

L.J. Sun performed the experiments and wrote the manuscript. Dr. Yi. Lu for the assistance with the MD simulation. L.X. Zhang helped to draw the Figures. H.S. Dong, L. Yang, and L.X. Zhang helped revised the manuscript. J.F. Zhao, L.X. Zhang and Y.C. Song planned, supervised, and led the project.

COMPETING INTERESTS

The authors declare no competing interests.

ADDITIONAL INFORMATION

Supplementary information The online version contains supplementary material available at https://doi.org/10.1038/s41545-023-00262-w.

Correspondence and requests for materials should be addressed to Lunxiang Zhang or Jiafei Zhao.

Reprints and permission information is available at http://www.nature.com/reprints

Publisher's note Springer Nature remains neutral with regard to jurisdictional claims in published maps and institutional affiliations.